Analysis of the Efficiency of Surfactant-Mediated Stabilization Reactions of EGaIn Nanodroplets

Lauren R. Finkenauer,[†] Qingyun Lu,[†] Ilhem F. Hakem, [†] Carmel Majidi,[§] Michael R. Bockstaller[†]*

†Department of Materials Science and Engineering, Carnegie Mellon University, 5000 Forbes Avenue, Pittsburgh, Pennsylvania, 15213, United States

§Department of Mechanical Engineering, Carnegie Mellon University, 5000 Forbes Avenue, Pittsburgh, Pennsylvania, 15213, United States

*) bockstaller@cmu.edu Tel.: ++1 412 268 2709; Fax.: ++1 412 268 7247

ABSTRACT

A methodology based on light scattering and spectrophotometry was developed to evaluate the effect of organic surfactants on the size *and* yield of eutectic gallium/indium (EGaIn) nanodroplets formed in organic solvents by ultrasonication. The process was subsequently applied to systematically evaluate the role of head-group chemistry as well as polar/apolar interactions of aliphatic surfactant systems on the efficiency of nanodroplet formation. Ethanol was found to be the most effective solvent medium in promoting the formation and stabilization of EGaIn nanodroplets. In ethanol, only thiol-based surfactants were found to promote the stabilization of nanodroplets. The yield of nanodroplet formation increased with the number of carbon atoms in the aliphatic part. In the case of the most effective surfactant system – octadecanethiol – the nanodroplet yield increased by about 370% as compared to pristine ethanol. The rather low overall efficiency of the reaction process along with the incompatibility of surfactant-stabilized EGaIn nanodroplets in nonpolar organic solvents suggests that the stabilization mechanism differs from the established self-assembled monolayer formation process that has been widely observed in nanoparticle formation processes.

Keywords: liquid metal, nanodroplets, surfactant, light scattering, EGaIn

INTRODUCTION

When dispersed in a soft carrier medium, nanoscale droplets of low temperature metals or alloys can be used to tailor the electronic, optical or thermal properties of the host material without significantly altering its elasticity or rheology. These liquid metal (LM) dispersions represent an intriguing platform for developing functional nanocomposite materials that manage electricity, electric field, and heat in biomechanically compatible machines and polymer electronics. To match the mechanical properties of natural human tissue, such composites must exhibit low-modulus (~0.1-1 MPa) elastic deformation up to large strains (>100%) and accommodate large bending and torsional deformations. This combination of mechanical, electrical, and thermal properties is difficult to accomplish with dispersions of rigid particle filler in a soft polymer due to internal mechanical mismatches that lead to mechanical hysteresis, stiffening, and embrittlement of the polymer matrix.[1] Recent advances in the development of low temperature eutectic alloy compositions have rendered liquid metal filler inclusions an attractive alternative to solid particle fillers.[2] Of particular interest has been eutectic gallium/indium (EGaIn) alloys that exhibit a eutectic melting temperature (at 1 bar) of $T = 15.3^{o}$C. For example, Ga-based LM alloys embedded in polymers have been used to create numerous types of devices such as a variety of antennas to include patch,[3] coil[4,5] and reconfigurable[6–8] structures, or tunable split-ring resonator;[9] compliant electrodes[3,10–15] for circuits and actuators[16–18]; a multitude of compliant and robust pressure[19,20] and strain sensors.[4,19,21,22] Self-healing capabilities have been demonstrated for extensible wires[23] and electrodes,[24] as well as soft composites.[25] Dispersion of liquid metal microdroplets in elastomeric matrices has led to elastic composites with LM inclusions and tunable electronic properties.[26,27]

While the applications listed above illustrate the potential of polymer-LM composites as a platform for material innovations, current fabrication processes also present constraints that limit the application of this new class of hybrid materials. In particular, current fabrication methods depend on the direct dispersion of liquid metal inclusions by mechanical (and/or sonic) mixing methods. This technique results in poor control of the dispersion morphology and leads to irregularly shaped micron sized 'droplet' inclusions that give rise to pronounced optical scattering and hence opaque materials.[28] To reduce scattering losses and to enable the integration of liquid-metal based nanocomposites into optically transparent coatings (e.g. for use in polymer photovoltaics), research has focused on the development of surfactant-stabilization methods. Tethering of surfactants to the surface of inorganic (or organic) nanoparticles is ubiquitously being used in nanomaterial synthesis.[29] The approach rests on surfactant binding to inhibit mass transport across the liquid/particle interface (thereby preventing particle growth) as well as to induce interactions that prevent particle aggregation and coagulation. Several previous studies have reported the use of surfactants to synthesize stabilized EGaIn (as well as other liquid metal) nanodroplets.[30–38] For example, Hohman *et al*. evaluated the sonochemical formation of EGaIn nanodroplet formation in the presence of 1-dodecanethiol (C12) and 3-mercapto-N-nonylpropionamide (1ATC9).[32] The authors observed nanoparticles down to tens of nanometers formed in the surfactant solutions. Without surfactants present, rapid agglomeration was reported.[32] The stabilization of EGaIn nanodroplets was interpreted as a consequence of chemisorption of sulfur atoms with gallium and/or indium at the surface. This might indeed be expected given the strong bond dissociation energy of Ga-S and In-S bonds which are on the order of 300 kJ/mol.[39] The authors also noted that minor amounts of oxygen supported particle stabilization. This was attributed to surface oxidation promoting the formation of wrinkles and

instabilities of the skin layer during sonication (a yield of 50 – 150 μg/mL for particles capped with 1-dodecanethiol was reported).[32] We note that the conclusions of this previous work were confirmed in the present study; specifically, some oxygen content was found to be necessary to induce particle stabilization (see Fig. S4). More recently, Lin *et al.* reported on the use of charged macromolecular surfactants control both size and shape of EGaIn nanostructures (demonstrating both nanosized spheres and rods).[38] Sudo *et al*. sonicated gallium in chloroform with both dodecanoic acid and dodecanamine as a surfactant, resulting in TEM observed particles of approximately 20 nm.[36] Consistent with observations by Hohman *et al*., no surfactant resulted in aggregated structures. Kramer and coworkers sonicated EGaIn particles in neat ethanol with and without the presence of SAM forming 1ATC9.[30] Drop casted particles subjected to "mechanical sintering" tests revealed that thiol capped particles ruptured more easily than oxide covered particles (no thiol), suggesting a lower surface tension of thiol capped compared to gallium oxide coated particles. The results highlight that the mechanism of surfactant stabilization remains an outstanding question. Harnessing surfactant-based synthesis for the fabrication of LM-based nanocomposite materials depends on a better understanding of the role of surfactants on the particle stabilization process. Here it is important to note that while previous studies have focused on the effect of surfactant on the size of nanodroplets, no systematic evaluation of the *efficiency* of nanodroplet formation (that is the yield of surfactant-mediated synthesis) has been reported. We attribute the lack of data on reaction efficiency to the difficulty of evaluating nanodroplet concentrations using established methods such as gravimetry that arise from the typically small amounts of material (see below).

The purpose of the present contribution was to systematically evaluate the role of surfactant composition on the size *and* yield of surfactant-mediated EGaIn nanodroplet formation.

Concurrent ultraviolet – visible (UV/Vis) absorption spectrophotometry and dynamic light scattering was applied to quantitatively determine size and size distribution of nanodroplets as well as EGaIn mass concentration. In agreement with previous reports, thiol-based surfactants were found to be most effective in stabilizing nanosized eutectic gallium/indium droplets. The efficiency was found to increase with the fraction of unpolar (aliphatic) groups, hence the yield of nanodroplet formation increased by 37% for 1-octadecanethiol as compared to the 1-dodecanethiol analog. Interestingly, the quantitative comparison of the effectiveness of nanodroplet formation in the presence/absence of surfactants revealed a 'threshold' chain length of the aliphatic moiety to enhance nanodroplet formation. A second interesting finding is that while the yield of nanodroplet formation increased by 340% (in the case of the most efficient surfactant system 1-octadecanethiol) compared to neat solvent, the overall efficiency of the process is found to be rather modest. This, in conjunction with the poor solubility of surfactant-stabilized nanodroplets, suggests that the mechanism of surfactant stabilization is more complex as previously noted and distinct from stabilization by 'self-assembled monolayer formation' process that has been proposed for other metal particle metal particle systems.[30,32,34,36,40]

The structure of the paper is as follows: First, the analytic process of determining the characteristics and yield of EGaIn nanodroplet products using optical spectrophotometry is described. Second, the role of solvent characteristics (polarity and ability to form hydrogen bonds) on the stabilization of EGaIn nanodroplets is discussed. In a third part, a systematic evaluation of the effect of chemical composition (*i.e.* type of functional groups) and length of unpolar residues on the size and yield of EGaIn nanodroplet formation during sonochemical synthesis will be reported for a range of aliphatic surfactants.

EXPERIMENTAL METHODS

EGaIn Synthesis Raw gallium (Ga) and indium (In) (99.99% pure, Gallium Source LLC) were combined to form the eutectic composition (75.5% Ga, 24.5% In by weight). The glass jar containing the metals and a magnetic stir bar was placed on a hot mixing plate at about 200°C until the alloy appeared thoroughly mixed. Direct scanning calorimetry was then used to verify that the alloy was indeed the eutectic of Ga-In. The melting temperature was determined as 16.35°C, which is within a 1°C range from the literature cited T_m of EGaIn (15.3°C). Once confirmed as the eutectic, approximately 1.5 mL of EGaIn was pulled into a syringe that was first repeatedly drawn with nitrogen. The liquid metal was then injected into a capped borosilicate glass vial through the septa. The vial was flushed with nitrogen for 5 minutes prior to the addition of EGaIn, which in additional to first purging the syringe, greatly reduced initial oxide formation (as evidenced by the resultant shiny metallic surface of the EGaIn within the vial). As a final precaution against oxygen "contamination," the caps were tightly wrapped with a layer of Parafilm M.

EGaIn Nanoparticle Synthesis Solutions of various selected surfactants were prepared in ethanol (200 proof, Anhydrous) at 1 mM concentrations and filtered three times (0.45 μm pore, PTFE membrane, PALL Acrodisk). From the given surfactant solution of interest, 1.5 mL was extracted and pipetted into a 2 mL borosilicate vial. Nitrogen was bubbled through the solution for 5 minutes to remove much of the dissolved oxygen. A syringe was then used to extract approximately 0.2 mg of EGaIn and inject it into the vial of surfactant solution. The vial was then capped, wrapped with Parafilm M, and placed in a secondary 120 mL polypropylene containment jar which was half filled with deionized water. A Branson 1510 bath ultrasonicator was filled with the same deionized water, and the jar was suspended in the center of the bath with the aid of a custom cut acrylic plate. The jar was sonicated at a continuous 40 kHz for 60 minutes (water initially at ~25°C,

with no additional temperature control). The bath was replaced after each synthesis to avoid temperature changes due to sonication. After sonication, the vial was removed from within the jar and allowed to decant for 24 hours in an upright position. Exactly 1.0 mL of supernatant was then pipetted away and introduced to a disposable semi-micro cuvette and used directly for testing.

Characterization Dynamic light scattering (DLS) was performed on samples after 24, 48 and 72 hours following their initial decanting process. A Malvern Zetasizer Nano ZS was used to record the scattering intensity autocorrelation function $g_2(q,t)$ at a scattering vector $q = 4\pi n\lambda^{-1}\sin(\theta/2) = 2.72 \times 10^7$ m^{-1} where n is the medium refractive index, $\lambda = 633$ nm is the vacuum wavelength of the incident light, corresponding to a scattering angle of $\theta = 173^\circ$ (converted to radians for q).

$$g_2(q,t) = \frac{\langle I(q,0)\, I(q,t)\rangle}{\langle I(q,0)\rangle^2} \tag{1}$$

$I(q)$ is the scattering intensity at a scattering vector q. The Siegert relation is used to compute the normalized autocorrelation function of the scattered electric field $g_1(q,t)$

$$g_2(q,t) = 1 + f^*|\alpha g_1(q,t)|^2 \tag{2}$$

where f* is an experimental instrument factor (determined by calibration), and α is the fraction of total scattered intensity stemming from fluctuations with correlation times longer than 10^{-7}s. The experimental $C(q,t) = \alpha g_1(q,t)$ describes the dynamics of the concentration fluctuations. A number size distribution representing the polydispersity of the sample was determined by the Malvern software, which was converted from the intensity size distribution using Mie theory.

UV/Vis spectroscopy was performed using a Cary UV/Vis 300 spectrophotometer (Agilent Technologies) on each sample to measure percent absorbance by suspended EGaIn nanoparticles. Experiments were performed over a wavelength range of 800 – 200 nm, with an interval of 1.0 nm

and a scan rate of 600 nm/min in double beam mode with the spectral band width (SBW) set at 2.0 nm. The experimental extinction A was determined using Beer-Lambert's law as $A = -\log_{10}(I/I_0)$ where I and I_0 represent the intensity of the transmitted and incident light, respectively.

Transmission electron microscopy (TEM) was performed on a JEOL 2000EX operated at 200 keV.

Calculation of the Extinction Cross Section of Nanoparticles The scattering and extinction cross section of EGaIn nanoparticles was determined using Mie theory for homogenous spheres. Calculations were performed using a following the procedure detailed by Bohren and Huffman.[41] Specifically, the expression for the extinction cross section (C_{ext}) is given by

$$C_{ext} = \frac{2\pi}{k^2}\sum_{n=1}^{\infty}(2n+1)\mathrm{Re}\{a_n + b_n\} \tag{3}$$

for which k is a wave vector[41] and a_n and b_n are the Mie scattering coefficients that are defined in terms of Riccati-Bessel functions of order n $\Psi_n(z)$, $\chi_n(z)$, $\zeta_n(z)$ as

$$a_n = \frac{\psi_n'(y)\psi_n(x) - m\psi_n(y)\psi_n'(x)}{\psi_n'(y)\zeta_n(x) - m\psi_n(y)\zeta_n'(x)} \tag{4}$$

$$b_n = \frac{m\psi_n'(y)\psi_n(x) - \psi_n(y)\psi_n'(x)}{m\psi_n'(y)\zeta_n(x) - \psi_n(y)\zeta_n'(x)} \tag{5}$$

Here, m is the ratio of the (complex) refractive index of the particle to the medium or N^*/N_m, where $N^* = N + iK$ is the complex refractive index of the EGaIn particle, x is wave vector k multiplied by radius of the sphere a or equivalently $x = ka = 2\pi N_\mathrm{m}a/\lambda$, and $y = mka = 2\pi N^* a/\lambda$ (where λ is wavelength). For numerical evaluation the sum was truncated at n_{max} iterations defined by Bohren and Huffman[41] to as $n_\mathrm{max} = x + 4x^{1/3} + 2$.

RESULTS AND DISCUSSION

To evaluate the role of surfactant composition on the formation of EGaIn nanodroplets a library of aliphatic surfactant systems with varying chemistry of head group and amphilicity were considered. Thiol-surfactants were considered because of the strong affinity of sulfur to a wide range of transition metals.[32,42] Amine and carboxyl-surfactants were considered because of their expected affinity to oxides since partial oxidation was hypothesized to play a role in EGaIn nanodroplet formation in the literature.[33,36,42] Aliphatic groups were considered because of the reported effectiveness of aliphatic surfactants in stabilizing EGaIn nanodroplets[32,33] as well as to enable the select evaluation of the role of amphilicity at otherwise constant chemical constitution. Table 1 summarizes the distinct surfactant systems that were considered in the present study.

Table 1. List of surfactants selection for variation study, along with ligand identifier, chemistry (functional group) and molecular weight. All surfactants used at 1.0 mM in ethanol.

Surfactant	Identifier	Functionality	M_w (g/mol)
$C_{18}H_{37} - SH$	C18	thiol	286.56
$C_{12}H_{25} - SH$	C12	thiol	202.40
$C_8H_{17} - SH$	C8	thiol	146.29
$C_4H_9 - SH$	C4	thiol	90.19
$C_{10}H_{21} - NH_2$	N10	amine	157.30
$C_8H_{17} - NH_2$	N8	amine	129.24
$C_{17}H_{35} - COOH$	SA	carboxylic acid	284.48
$C_{11}H_{23} - COOH$	DA	carboxylic acid	200.32

All tests were conducted at a concentration of 1mM surfactant in ethanol (EtOH) solution at 293 K. This corresponds to reaction conditions that were previously reported as being 'most effective' for the stabilization of EGaIn nanodroplets. To validate the conclusion of previous reports, solvent variation tests were performed (see Fig. S1) in which the formation of EGaIn nanodroplets was evaluated in polar protic solvents (water, methanol, ethanol, isopropyl alcohol) as well as polar aprotic (dimethylformamide, dimethylsulfoxide) and unpolar solvents (toluene). Among all solvents, the analysis of nanodroplet formation (using the experimental procedures described below) was observed to be most effective in ethanol. Although the yield in ethanol was found to be approximately equal to isopropanol (IPA) (see Fig. S1), ethanol solutions consistently resulted in unimodal particle size distributions, as opposed to bimodal size distributions that were observed when performing the reactions in IPA (see Fig. S2). While the origin for the particular efficiency of ethanol is not currently known, we hypothesize that it might be related to the solvation capability of ethanol that suppresses the formation of micellar aggregate structures of surfactants in solution (the latter was confirmed by dynamic light scattering on surfactant solutions). Similarly, the variation of the concentration of mercaptododecane in ethanol within the range 1 – 10 mM revealed no improvement of nanodroplet formation at concentrations higher than 1 mM $C_{12}H_{25}SH$ (see Fig. S3). This confirms prior reports by Hohman and coworkers who identified a surfactant concentration of 1 mM as 'optimum' for nanodroplet synthesis and thus provides the rationale for the reaction conditions that were chosen for the comparative surfactant evaluation that is the subject of the present paper.[32]

To induce nanodroplet formation, ~0.2 mg of EGaIn was mixed with 1.5 mL of surfactant solution. The mixtures were subsequently sonicated for 60 minutes at 40 kHz as described in the literature. To evaluate the role of surfactants on nanodroplet formation all reactions were carried

out multiple times under identical conditions to ascertain the reproducibility of reactions. Values reported for efficiency and particle size thus represent average values calculated on the basis of three experiments. Because gravimetric methods were found to be impractical for determining the yield of nanodroplet formation, an optical characterization process based on the quantitative analysis of the scattering strength of nanodroplet solutions was employed instead. The process is composed of three steps: First, the determination of particle size distributions using dynamic light scattering (DLS). Second, the measurement of the extinction coefficient of nanodroplet solutions using UV/Vis spectrophotometry. Finally, the yield was deduced by analysis of the total scattering strength of nanodroplet solutions with a Mie model[41,43] for EGaIn spheres with corresponding size distribution. Figure 1 depicts the experimental field autocorrelation function $C(q, t)$ measured at $q = 2.72 \times 10^7\ m^{-1}$, 24 hrs after sonication of EGaIn dispersion in EtOH/$C_{12}H_{25}SH$. The high quality of the dispersion is evident by the excellent fit of $C(q, t)$ with a single exponential function. Contin analysis of $C(q, t)$ was used to determine the number-weighted particle size distribution $P_n(D_H)$ where D_H denotes the hydrodynamic diameter of particles (the fit as well as residuals are shown in Figure 1).

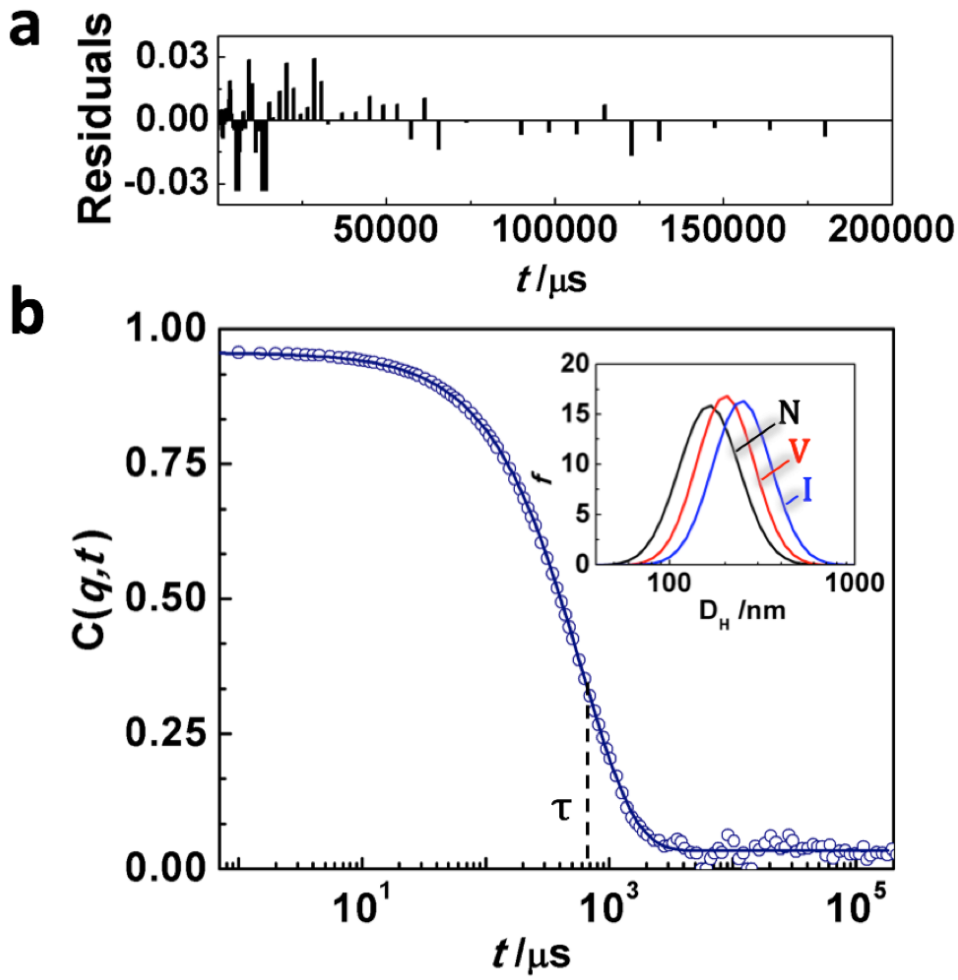

Figure 1. Representative light scattering results of EGaIn nanodroplets in EtOH/$C_{12}H_{25}SH$ (see text for more details). Figure shows experimental autocorrelation function of the electric field $C(q, t)$ measured at $q = 2.72 \times 10^7$ m^{-1}, 24 hrs after sonication along with Contin fit. Inset in main figure shows number (N, black), volume (V, red), and intensity (I, blue) weighted distributions of hydrodynamic diameters that were determined through Contin analysis. Top panel shows random variation of residuals thus confirming the high quality of fit.

Since hydrodynamic interactions in suspensions of spheres are expected to be negligible if the distance between adjacent particles is larger than the particle size, *i.e.* in the limit of $(V/N_p)^{1/3} >> D$ (where $(V/N_p)^{1/3}$ denotes the average distance between spheres in the suspension for volume V, total number of particles N_p and sphere diameter D), the hydrodynamic size is in the following assumed to be equal to the geometric diameter of EGaIn particles. The proximity of number, weight and intensity weighted distributions (shown in the inset of Figure 1) confirms the narrow size distribution of nanodroplets. To validate the results from DLS analysis, the particle size of select systems was concurrently evaluated using transmission electron microscopy (TEM).

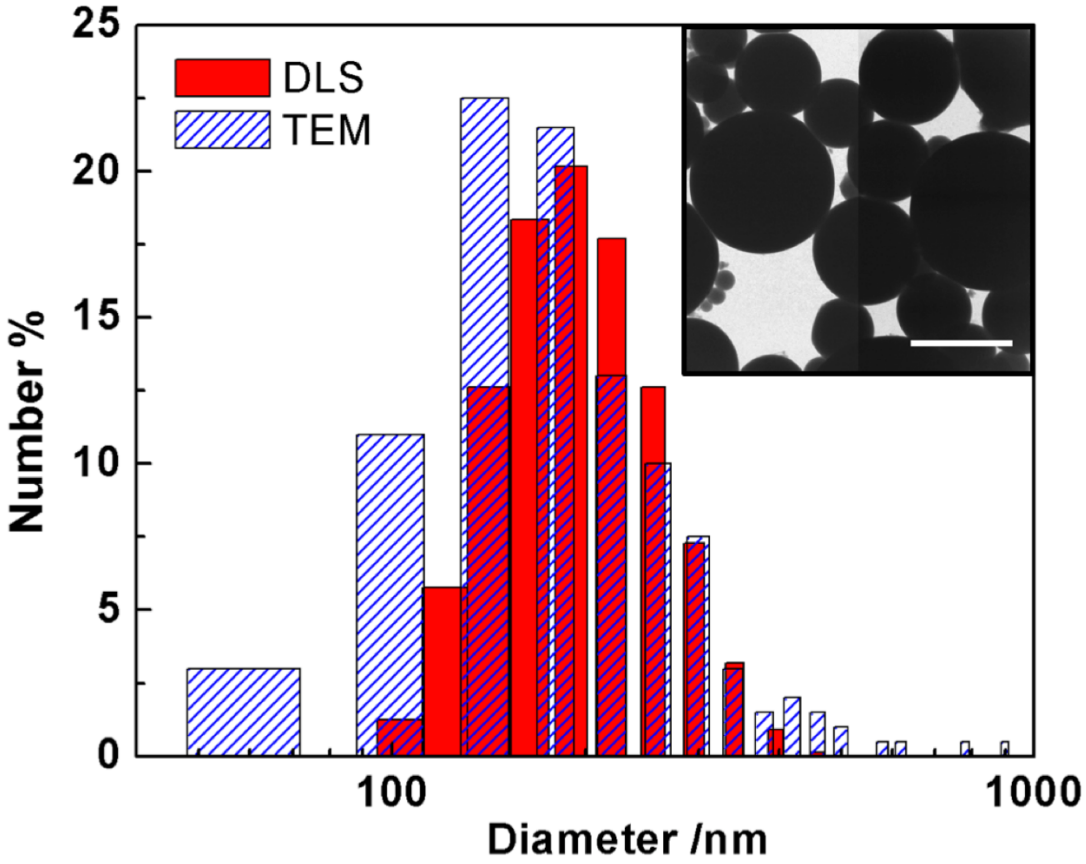

Figure **2** depicts the corresponding number weighted size distribution $P_n(D)$ along with the corresponding size distribution determined by TEM analysis for the EGaIn/$C_{12}H_{25}SH$ system. The agreement between the respective average values $\langle D \rangle_{DLS} \approx 176$ nm and $\langle D \rangle_{TEM} \approx 150$ nm confirms

the DLS analysis. Because light scattering is a bulk characterization method that allows the rapid evaluation of macroscopic material volumes, DLS analysis was used to determine size distributions of EGaIn nanodroplets in suspension.

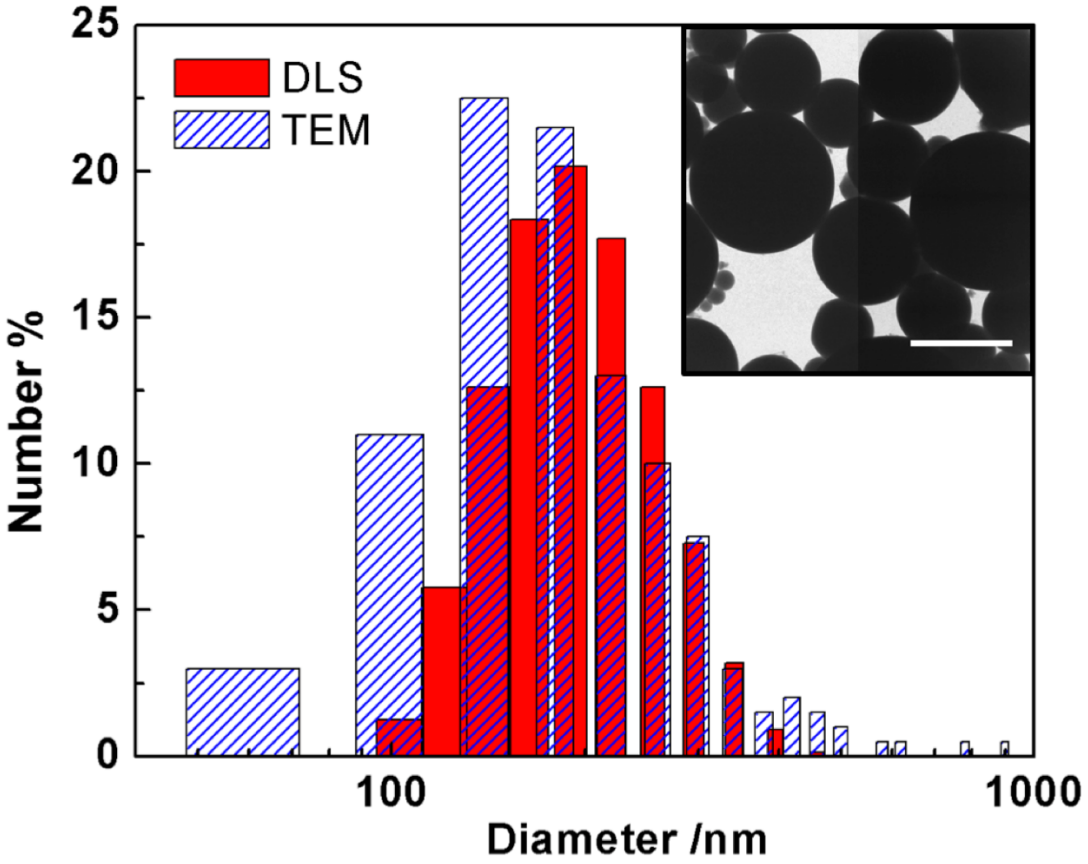

Figure 2. Comparison of DLS software provided number size distribution with $\langle D_{\mathrm{TEM}} \rangle \approx 150$ nm for dodecanethiol thiol sample at 24 hours with particle size distribution for dodecanethiol sample determined from 200 particles using electron microscopy where $\langle D_{\mathrm{DLS}} \rangle \approx 176$ nm. Inset is TEM micrograph of sample showing range of particles consistent with distributions. Scale bar 500 nm.

To quantitatively relate the size distribution of EGaIn nanodroplets to the extinction coefficient of nanodroplet suspensions, calculations of the average extinction cross section of

disperse spherical nanodroplets using Mie theory were performed. A prerequisite for performing these calculations is knowledge of the optical constants N and K that represent the real and imaginary part of the refractive index of EGaIn nanodroplets, respectively. Optical constants were determined from tabulated values of indium and gallium using the effective medium method.[44,45] The latter has been shown to provide adequate representation of the optical and dielectric properties of uniform atomic solutions of components that are expected for EGaIn above the eutectic temperature. Thus, the effective dielectric constant was calculated using Newton's formula which represents a simple volume-weighted average of the dielectric properties of the constituents, *i.e.* $\varepsilon_{eff} = \phi\varepsilon_1 + (1-\phi)\varepsilon_2$, where ϕ denotes the volume fraction and ε_i the dielectric constant of component i. This homogenization model has been shown to provide adequate representations of the dielectric properties of multicomponent systems that are mixed on the atomic level (such as liquid metal alloys).[45] Dielectric values determined following to this process were also consistent in trend and order of magnitude with previously reported values by Morales *et al.* on the basis of electrochemical properties of oxide surfaces.[46] Optical constants were subsequently calculated based on the relations $\varepsilon_{eff}' = N^2 - K^2$ and $\varepsilon_{eff}'' = 2NK$ where ε_{eff}' and ε_{eff}'' represent the real and imaginary part of the effective dielectric constant, respectively. Figure 3 illustrates the trends of N and K of EGaIn nanodroplets that were determined based on an effective medium theory along with the respective optical constants of the constituent components.

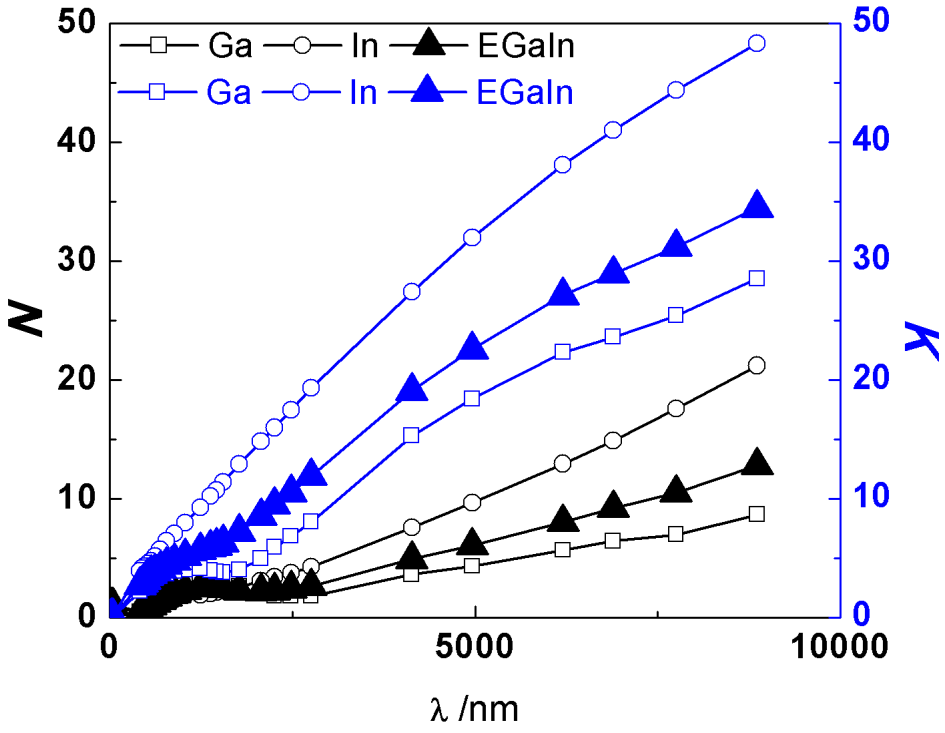

Figure 3. Real (*N*) and imaginary (*K*) components of the refractive index for EGaIn as determined from effective medium approximations compared with known values for Gallium and Indium as a function of wavelength. See text for full detail.

It is noted that the process for calculating the optical constants that is outlined above neglects any effect due to the finite size on the optical constants of EGaIn nanodroplets. Size effects on the optical properties of metal nanoparticles have been shown to primarily result from classical surface scattering of electrons that arises if the size of particles decreases below the electron mean free path (except for the limit of very small particle size where quantization effects can occur).[47] Since

the electron mean free path in metals is typically of the order of 20 nm, *i.e.* much less than the average size of EGaIn nanodroplets, bulk properties can safely be assumed in the present case.

The extinction cross section of disperse nanodroplets was subsequently determined as

$$\langle C_{\text{ext}}(\lambda)\rangle = \int C_{\text{ext}}(D,\lambda)P_n(D)\,\mathrm{d}D \Big/ \int P_n(D)\,\mathrm{d}D \tag{6}$$

using Mie theory (see eqs. 3 – 5) where the denominator in eq. 6 equals to one if $P(D)$ is normalized.[48] From the experimental extinction A (see 'Experimental Methods' section) the number of EGaIn nanodroplets was then determined via $N_p = 2.303AV\langle C_{\text{ext}}(\lambda^*)\rangle^{-1}l^{-1}$, where $\langle C_{\text{ext}}(\lambda^*)\rangle$ is the average extinction cross section for the corresponding particle distribution $P_n(D)$ at a test wavelength λ^*, l = 1 cm is the pathlength and V is the sample volume. The test wavelength was chosen to be λ^* = 505 nm for reasons of practicality (*i.e.* good signal-to-noise ratio with no interference by solvent or surfactant components). We note that the choice of λ^* introduces some ambiguity with regards to the uniqueness of the result; however, based on the good agreement between experimental and calculated A (see below) the error associated with any particular choice of λ^* (in the range of 450 nm < λ^* < 600 nm) is expected to be less than 5%. We further note that for calculation of the extinction cross section, the refractive index of the solvent medium was assumed to be equal to the value of pristine EtOH ($N_{\text{EtOH}} = N_0 = 1.3616$ at λ = 500 nm and T = 20 °C). The neglect of surfactant contributions to the refractive index is not expected to result in relevant errors due to the small surfactant concentration of 1 mM. To assess the validity of the process to determine the number density of suspended particles, measurements of reference solutions of colloidal silica of known concentration were performed (see Fig. S5); the accuracy of the method was found to be within 20 wt%. Figure 4 displays the experimental extinction of EGaIn nanodroplets in EtOH/$C_{12}H_{25}SH$ solution along with the calculated extinction (for $N_p = 5.7 \times 10^8$).

The figure reveals excellent agreement between calculated and experimental values across most of the visible wavelength range. Note that good agreement is only achieved by accounting for particle size dispersity. This is illustrated in the inset of Figure 4 that depicts the respective scattering and absorption cross sections of EGaIn nanodroplets assuming a uniform size equal to the average droplet diameter (*i.e.* $D = \langle D \rangle$) (red symbols) as well as for a size distribution corresponding to $P_n(D)$ (blue symbols).

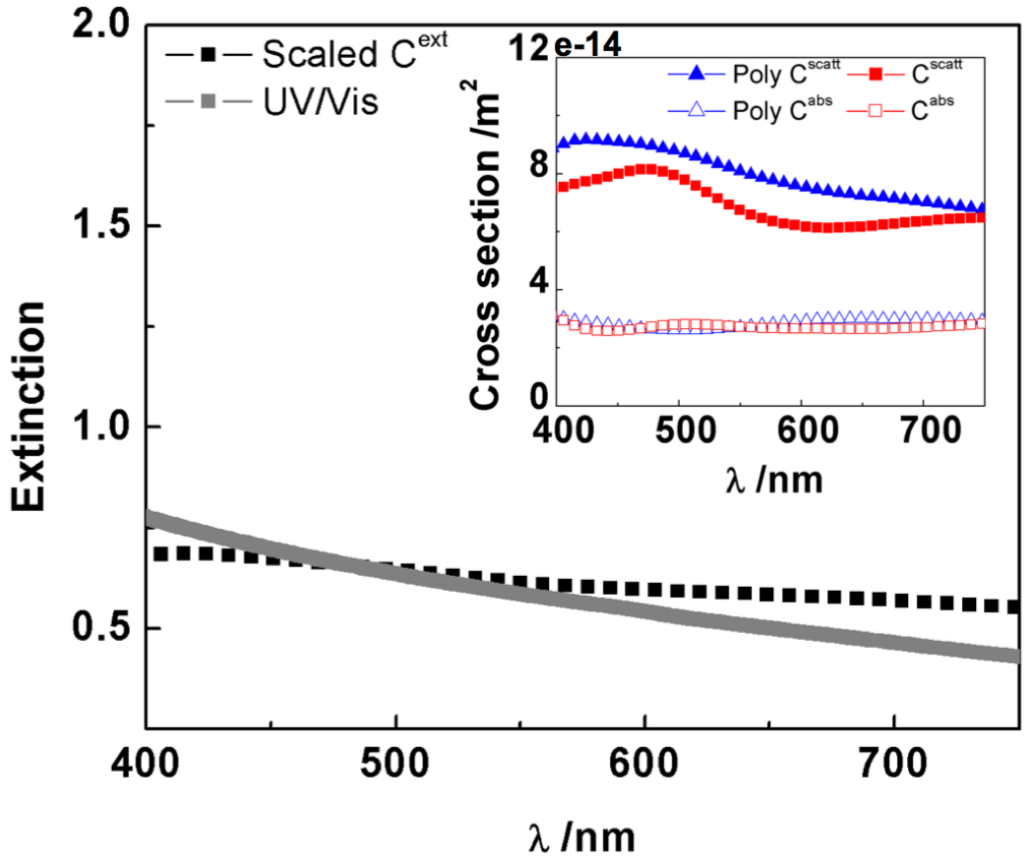

Figure 4. Extinction as a function of wavelength for the visible spectrum from raw UV/Vis data and scaled extinction coefficient data calculated from eqs. 3-6. Inset shows the scattering and absorption cross sections for the case of a uniform particle size compared to a disperse distribution. Triangles correspond to cross sections accounting for polydispersity, while squares are results

assuming a monodisperse system. Filled and open symbols represent scattering and absorption cross sections, respectively.

Comparison of the scattering (filled symbols) and absorption (open symbols) cross sections also reveals that the optical extinction of EGaIn nanodroplet solutions is dominated by the scattering of nanodroplets. This supports previous reports on the optical properties of metal nanoparticles that have shown that the scattering cross section typically exceeds the absorption cross section for particle diameter exceeding 20 nm (the latter can be rationalized as a consequence of the distinct dependences of the cross sections on the particle volume, *i.e.* $C^{scatt} \sim V_p^2$ and $C^{abs} \sim V_p$).[28,45,49,50]

Figure 5 depicts the number average particle diameter $\langle D \rangle$ of EGaIn nanodroplets that was determined from the particle size distributions (via $\langle D \rangle = \int D P_n(D) dD$). Average particle diameter ranged from $\langle D \rangle$ = 80 nm for $C_{18}H_{37}SH$ to $\langle D \rangle$ = 250 nm for stearic acid solutions. Note that the result for dodecanethiol $\langle D \rangle$ = 170 nm closely matches the results reported by Hohman *et al*. who first reported the surfactant mediated synthesis of EGaIn nanodroplets.[32] A pertinent feature that is revealed by Figure 5 is that nanodroplet formation also occurs in pristine EtOH solution*, i.e.* in

the absence of surfactant additives. For all solution systems nanodroplet size was found to be stable for 72 hours (the exception being stearic acid which showed a decreasing particle size).

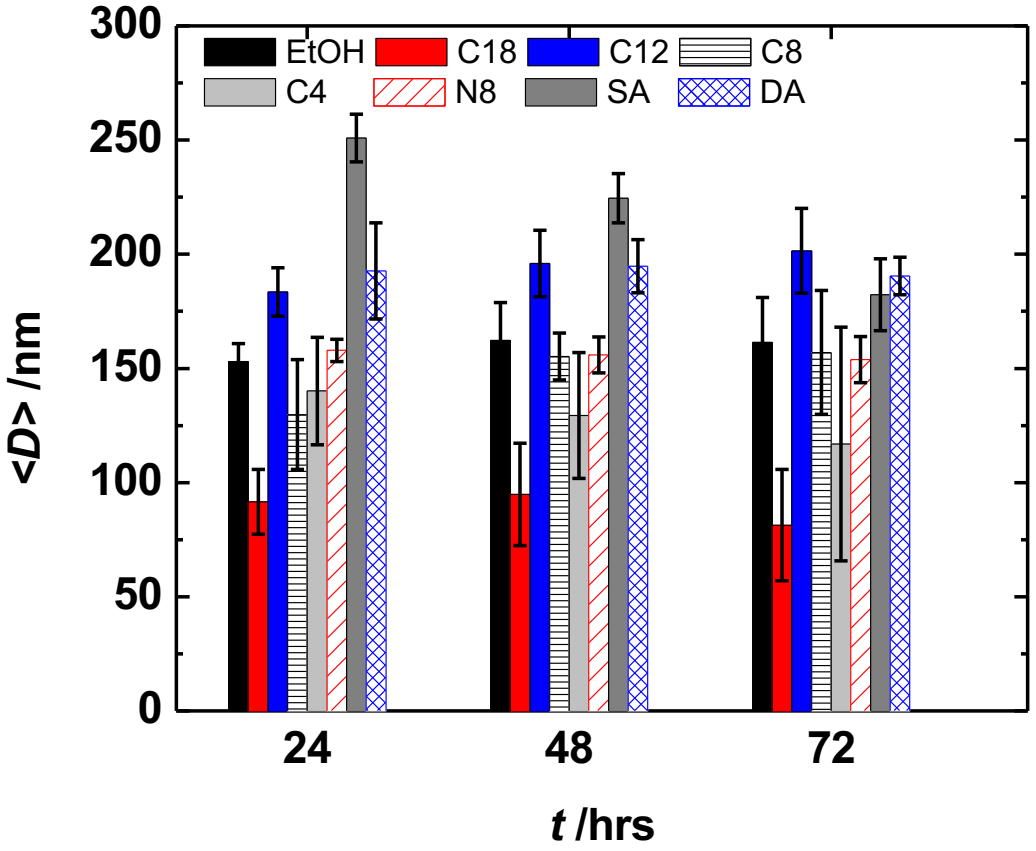

Figure 5. EGaIn particle size evolution over three days for various surfactants in 1 mM ethanol solutions compared against neat ethanol (EtOH). C8 = octanethiol, C12 = dodecanethiol, C18 = octadecanethiol, C4 = butanethiol, N8 = octylamine, SA = "stearic acid" or octadecanoic acid, DA = dodecanoic acid. Error bar is standard deviation for n = 3.

It is important to note that, because nanodroplet formation is also observed in pristine EtOH, the evaluation of droplet size is not sufficient to assess the benefit of surfactant addition but rather the yield of droplet formation has to be determined. The total mass of EGaIn nanodroplets dispersed

in surfactant solutions was determined from the experimental number density of EGaIn droplets as $m_{\mathrm{EGaIn}} = N(4\pi/3)\rho_{\mathrm{EGaIn}}\int (D/2)^3 P_n(D)dD$ where ρ_{EGaIn} = 6.25 g/mL is the density of EGaIn and normalization of $P_n(D)$ has been assumed. **Error! Reference source not found.** displays the resulting EGaIn concentrations as molarity (c_{EGaIn} = mmol EGaIn per liter solvent) at 24 hrs, 48

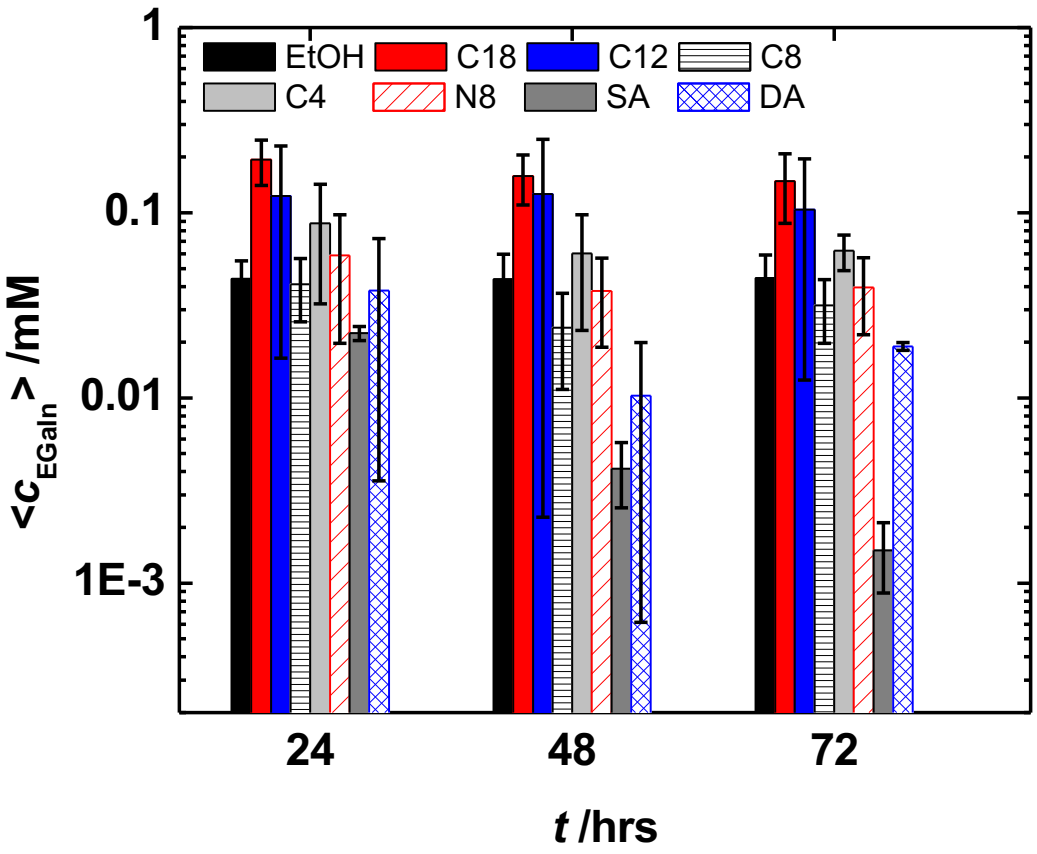

hrs, and 72 hrs after sonication.

Figure 6. EGaIn concentration evolution over three days for various surfactants in 1 mM ethanol solutions compared against neat ethanol (EtOH). C8 = octanethiol, C12 = dodecanethiol, C18 = octadecanethiol, C4 = butanethiol, N8 = octylamine, SA = "stearic acid" or octadecanoic acid, DA = dodecanoic acid. Error bar is standard deviation for n = 3.

Figure 6 reveals several pertinent features: First, mercapto-based surfactants display higher yields for nanodroplet formation as compared to alternative solvent systems. Second, of the different aliphatic surfactant systems tested in the present study, mercapto-octadecane exhibits the highest yield of nanodroplet formation, exceeding the yield of mercapto-dodecane – the previously mentioned most efficient aliphatic surfactant – by approximately 200%. The higher yield of $C_{18}H_{37}SH$ (as compared to $C_{12}H_{25}SH$) is also associated with a smaller droplet size ($\langle D \rangle$ = 80 nm *vs* 170 nm). The latter should be of interest from an application perspective. In both $C_{18}H_{37}SH$ and $C_{12}H_{25}SH$, the concentration and size of droplets was found to be stable within the 72-hour time interval tested in the present study. Interestingly, the quantification of nanodroplet yield also reveals that most surfactant systems do not improve nanodroplet formation in any statistically relevant amount. Even for $C_{12}H_{25}SH$, the more significant experimental uncertainty renders a determination difficult. Only for $C_{18}H_{37}SH$ is the benefit of surfactant addition unequivocal, raising the yield of nanodroplet formation by over 300% as compared to pristine EtOH.

To further elucidate the mechanism of surfactant addition on EGaIn nanodroplet formation, dispersed nanodroplets were transferred to a variety of organic solvents. Rapid precipitation of EGaIn nanodroplets was observed in unpolar solvents. This suggested that the stabilization mechanism is not related to the formation of dense self-assembled monolayers that have been widely observed for metal particle systems.[51,52] We note that this subdued influence of surfactants is also consistent with the observation that the EGaIn nanodroplet diameter in the absence of surfactant is similar to those found in the presence of surfactants (see data for pure ethanol in Fig. 5).[37] Yamaguchi et al. maintained that $C_{12}H_{25}SH$ (as well native oxide formation) are important for regulating nanoparticle size and preventing coalescence for the case of Gallium nanodroplets.[34] Such reasoning might be extended to the present system and hence we suggest that the mechanism

of surfactant-enhanced synthesis involves the manipulation of the rate of oxide formation that could play an important role in preventing particle coagulation (by providing a mechanical barrier to droplet fusion). In this case, the increased yield of droplet formation in the presence of surfactant might be interpreted to be a consequence of the oxidation rate being slow enough to enable the efficient breakup of liquid during sonication but fast enough to prevent droplet fusion through partial oxidation. An interesting observation is that the effectiveness of thiol-surfactants was found to increase with surfactant molecular weight (with the exception of mercapto-butane). This influence of the surfactant molecular weight suggests that the exchange kinetics of surfactants may play a large role in oxide formation. Since longer chain aliphatic thiols have a reduced solubility than shorter surfactant molecules, longer chains are expected to exhibit longer interaction periods with particles. The different exchange kinetics should affect the rates of oxide formation and hence the dispersion stability of nanodroplet systems. Here we note that the formation of oxide layers could not be unequivocally demonstrated for the systems used in the present study and thus a final determination of the mechanism cannot be offered at this point. Clearly, more research will be needed to better understand the role of surfactant addition on the stabilization of EGaIn nanodroplet formation.

CONCLUSIONS

An optical characterization approach based on concurrent dynamic light scattering and photospectrometry was applied to evaluate the efficiency of aliphatic surfactant systems to stabilize EGaIn nanodroplets during the sonication of dispersions. Nanodroplet formation was most significant in the presence of thiol-based surfactants, and mercapto-octadecane was found to

be the most effective surfactant system. The analytical process reveals that quantification of particle size alone is insufficient to determine the efficiency of surfactant based EGaIn nanodroplet synthesis since nanodroplet formation also occurs in the pristine solvent. Rather the mass of dispersed EGaIn should be considered as the relevant quantity to judge the efficacy of surfactant stabilization. Only in case of two surfactant systems (mercapto-dodecane and mercapto-octadecane) was the yield of nanodroplet formation found to exceed the one of the solvent beyond the error margin; mercapto-octadecane was found to be the most effective surfactant system. The results suggest that surfactants play a fundamentally different role in nanodroplet stabilization as in other metal particle systems where the formation of dense self-assembled monolayers has been widely observed. Future research should focus on the elucidation of the surface chemical composition and structure of EGaIn nanodroplets, for example, through the use of XP, to better understand the mechanism of surfactant-induced stabilization. It is hoped that the process presented in this contribution will assist in the development of facile synthesis processes towards EGaIn (and other low temperature and liquid metal) nanomaterials.

AUTHOR INFORMATION

The authors declare no competing financial interest.

ACKNOWLEDGMENT

This material is based upon work supported by the National Science Foundation Graduate Research Fellowship Program under Grant No. DGE1252522 and by the Air Force Office of Scientific Research under award number FA9550-16-1-0566. The authors further acknowledge

funding by the National Science Foundation via grant CMMI-1663305. Any opinions, findings, and conclusions or recommendations expressed in this material are those of the author(s) and do not necessarily reflect the views of the National Science Foundation. The authors also acknowledge one of the reviewers for their valuable discussion of the effect surfactant exchange kinetics on nanoparticle formation.

SUPORTING INFORMATION

Supporting information (additional experimental data on the role of solvent structure and oxygen content on EGaIn nanodroplet formation) is available and can be accessed via http://www.acs.org

REFERENCES

(1) Ojha, S.; Dang, A.; Hui, C. M.; Mahoney, C.; Matyjaszewski, K.; Bockstaller, M. R. Strategies for the Synthesis of Thermoplastic Polymer Nanocomposite Materials with High Inorganic Filling Fraction. *Langmuir* **2013**, *29* (28), 8989–8996.

(2) Kazem, N.; Hellebrekers, T.; Majidi, C. Soft Multifunctional Composites and Emulsions with Liquid Metals. *Adv. Mater.* **2017**.

(3) Hayes, G. J.; Ju-Hee So; Qusba, A.; Dickey, M. D.; Lazzi, G. Flexible Liquid Metal Alloy (EGaIn) Microstrip Patch Antenna. *IEEE Trans. Antennas Propag.* **2012**, *60* (5), 2151–2156.

(4) Fassler, A.; Majidi, C. Soft-Matter Capacitors and Inductors for Hyperelastic Strain Sensing and Stretchable Electronics. *Smart Mater. Struct.* **2013**, *22* (5), 55023.

(5) Lazarus, N.; Meyer, C. D.; Bedair, S. S.; Nochetto, H.; Kierzewski, I. M. Multilayer Liquid Metal Stretchable Inductors. *Smart Mater. Struct.* **2014**, *23* (8), 85036.

(6) Cheng, S.; Wu, Z. A Microfluidic, Reversibly Stretchable, Large-Area Wireless Strain Sensor. *Adv. Funct. Mater.* **2011**, *21* (12), 2282–2290.

(7) Wang, M.; Trlica, C.; Khan, M. R.; Dickey, M. D.; Adams, J. J. A Reconfigurable Liquid Metal Antenna Driven by Electrochemically Controlled Capillarity. *J. Appl. Phys.* **2015**, *117* (19), 194901.

(8) Koo, C.; LeBlanc, B. E.; Kelley, M.; Fitzgerald, H. E.; Huff, G. H.; Han, A. Manipulating Liquid Metal Droplets in Microfluidic Channels With Minimized Skin Residues Toward Tunable RF Applications. *J. Microelectromechanical Syst.* **2015**, *24* (4), 1069–1076.

(9) Liu, P.; Yang, S.; Jain, A.; Wang, Q.; Jiang, H.; Song, J.; Koschny, T.; Soukoulis, C. M.; Dong, L. Tunable Meta-Atom Using Liquid Metal Embedded in Stretchable Polymer. *J. Appl. Phys.* **2015**, *118* (1), 14504.

(10) Lipomi, D. J.; Vosgueritchian, M.; Tee, B. C.-K.; Hellstrom, S. L.; Lee, J. A.; Fox, C. H.; Bao, Z. Skin-like Pressure and Strain Sensors Based on Transparent Elastic Films of Carbon Nanotubes. *Nat. Nanotechnol.* **2011**, *6* (12), 788–792.

(11) So, J.-H.; Dickey, M. D. Inherently Aligned Microfluidic Electrodes Composed of Liquid Metal. *Lab. Chip* **2011**, *11* (5), 905.

(12) Pekas, N.; Zhang, Q.; Juncker, D. Electrostatic Actuator with Liquid Metal–elastomer Compliant Electrodes Used for on-Chip Microvalving. *J. Micromechanics Microengineering* **2012**, *22* (9), 97001.

(13) Richards, A. L.; Dickey, M. D.; Kennedy, A. S.; Buckner, G. D. Design and Demonstration of a Novel Micro-Coulter Counter Utilizing Liquid Metal Electrodes. *J. Micromechanics Microengineering* **2012**, *22* (11), 115012.

(14) Thredgold, L. D.; Khodakov, D. A.; Ellis, A. V.; Lenehan, C. E. On-Chip Capacitively Coupled Contactless Conductivity Detection Using "injected" Metal Electrodes. *The Analyst* **2013**, *138* (15), 4275.

(15) Hallfors, N.; Khan, A.; Dickey, M. D.; Taylor, A. M. Integration of Pre-Aligned Liquid Metal Electrodes for Neural Stimulation within a User-Friendly Microfluidic Platform. *Lab. Chip* **2013**, *13* (4), 522.

(16) Finkenauer, L. R.; Majidi, C. Compliant Liquid Metal Electrodes for Dielectric Elastomer Actuators; Bar-Cohen, Y., Ed.; 2014; p 90563I.

(17) Wissman, J.; Finkenauer, L.; Deseri, L.; Majidi, C. Saddle-like Deformation in a Dielectric Elastomer Actuator Embedded with Liquid-Phase Gallium-Indium Electrodes. *J. Appl. Phys.* **2014**, *116* (14), 144905.
(18) Rosset, S.; Shea, H. R. Flexible and Stretchable Electrodes for Dielectric Elastomer Actuators. *Appl. Phys. A* **2012**.
(19) Park, Y.-L.; Majidi, C.; Kramer, R.; Bérard, P.; Wood, R. J. Hyperelastic Pressure Sensing with a Liquid-Embedded Elastomer. *J. Micromechanics Microengineering* **2010**, *20* (12), 125029.
(20) Kramer, R. K.; Majidi, C.; Sahai, R.; Wood, R. J. Soft Curvature Sensors for Joint Angle Proprioception; IEEE, 2011; pp 1919–1926.
(21) Kramer, R. K.; Majidi, C.; Wood, R. J. Wearable Tactile Keypad with Stretchable Artificial Skin; IEEE, 2011; pp 1103–1107.
(22) Matsuzaki, R.; Tabayashi, K. Wearables: Highly Stretchable, Global, and Distributed Local Strain Sensing Line Using GaInSn Electrodes for Wearable Electronics (Adv. Funct. Mater. 25/2015). *Adv. Funct. Mater.* **2015**, *25* (25), 3797–3797.
(23) Palleau, E.; Reece, S.; Desai, S. C.; Smith, M. E.; Dickey, M. D. Self-Healing Stretchable Wires for Reconfigurable Circuit Wiring and 3D Microfluidics. *Adv. Mater.* **2013**, *25* (11), 1589–1592.
(24) Liu, Y.; Gao, M.; Mei, S.; Han, Y.; Liu, J. Ultra-Compliant Liquid Metal Electrodes with in-Plane Self-Healing Capability for Dielectric Elastomer Actuators. *Appl. Phys. Lett.* **2013**, *103* (6), 64101.
(25) Blaiszik, B. J.; Kramer, S. L. B.; Grady, M. E.; McIlroy, D. A.; Moore, J. S.; Sottos, N. R.; White, S. R. Autonomic Restoration of Electrical Conductivity. *Adv. Mater.* **2012**, *24* (3), 398–401.
(26) Fassler, A.; Majidi, C. Liquid-Phase Metal Inclusions for a Conductive Polymer Composite. *Adv. Mater.* **2015**, *27* (11), 1928–1932.
(27) Bartlett, M. D.; Fassler, A.; Kazem, N.; Markvicka, E. J.; Mandal, P.; Majidi, C. Stretchable, High- *K* Dielectric Elastomers through Liquid-Metal Inclusions. *Adv. Mater.* **2016**, *28* (19), 3726–3731.
(28) Dang, A.; Ojha, S.; Hui, C. M.; Mahoney, C.; Matyjaszewski, K.; Bockstaller, M. R. High-Transparency Polymer Nanocomposites Enabled by Polymer-Graft Modification of Particle Fillers. *Langmuir* **2014**, *30* (48), 14434–14442.
(29) Bishop, K. J. M.; Wilmer, C. E.; Soh, S.; Grzybowski, B. A. Nanoscale Forces and Their Uses in Self-Assembly. *Small* **2009**, *5* (14), 1600–1630.
(30) Boley, J. W.; White, E. L.; Kramer, R. K. Mechanically Sintered Gallium-Indium Nanoparticles. *Adv. Mater.* **2015**, 2355–2360.
(31) Pokroy, B.; Aichmayer, B.; Schenk, A. S.; Haimov, B.; Kang, S. H.; Fratzl, P.; Aizenberg, J. Sonication-Assisted Synthesis of Large, High-Quality Mercury Thiolate Single Crystals Directly from Liquid Mercury. *J. Am. Chem. Soc.* **2010**, *132* (41), 14355–14357.
(32) Hohman, J. N.; Kim, M.; Wadsworth, G. A.; Bednar, H. R.; Jiang, J.; LeThai, M. A.; Weiss, P. S. Directing Substrate Morphology via Self-Assembly: Ligand-Mediated Scission of Gallium–Indium Microspheres to the Nanoscale. *Nano Lett.* **2011**, *11* (12), 5104–5110.
(33) Tevis, I. D.; Newcomb, L. B.; Thuo, M. Synthesis of Liquid Core–Shell Particles and Solid Patchy Multicomponent Particles by Shearing Liquids Into Complex Particles (SLICE). *Langmuir* **2014**, *30* (47), 14308–14313.

(34) Yamaguchi, A.; Mashima, Y.; Iyoda, T. Reversible Size Control of Liquid-Metal Nanoparticles under Ultrasonication. *Angew. Chem.* **2015**, *127*, 1–6.
(35) Ren, L.; Zhuang, J.; Casillas, G.; Feng, H.; Liu, Y.; Xu, X.; Liu, Y.; Chen, J.; Du, Y.; Jiang, L.; et al. Nanodroplets for Stretchable Superconducting Circuits. *Adv. Funct. Mater.* **2016**.
(36) Sudo, S.; Nagata, S.; Kokado, K.; Sada, K. Direct Synthesis of Liquid Metal Colloids and Their Transmetalation into Noble Metal Nanoparticles. *Chem. Lett.* **2014**, *43* (8), 1207–1209.
(37) Lear, T. R.; Hyun, S.-H.; Boley, J. W.; White, E. L.; Thompson, D. H.; Kramer, R. K. Liquid Metal Particle Popping: Macroscale to Nanoscale. *Extreme Mech. Lett.* **2017**, *13*, 126–134.
(38) Lin, Y.; Liu, Y.; Genzer, J.; Dickey, M. D. Shape-Transformable Liquid Metal Nanoparticles in Aqueous Solution. *Chem Sci* **2017**, *8* (5), 3832–3837.
(39) *Lange's Handbook of Chemistry*, 11. ed.; Dean, J. A., Lange, N. A., Eds.; McGraw-Hill: New York, 1973.
(40) Han, Z. H.; Yang, B.; Qi, Y.; Cumings, J. Synthesis of Low-Melting-Point Metallic Nanoparticles with an Ultrasonic Nanoemulsion Method. *Ultrasonics* **2011**, *51* (4), 485–488.
(41) *Absorption and Scattering of Light by Small Particles*; Bohren, C. F., Huffman, D. R., Eds.; Wiley-VCH Verlag GmbH: Weinheim, Germany, 1998.
(42) Jadhav, S. A. Self-Assembled Monolayers (SAMs) of Carboxylic Acids: An Overview. *Cent. Eur. J. Chem.* **2011**, *9* (3), 369–378.
(43) Mie, G. Beiträge zur Optik trüber Medien, speziell kolloidaler Metallösungen. *Ann. Phys.* **1908**, *330* (3), 377–445.
(44) Adachi, S. *The Handbook on Optical Constants of Metals in Tables and Figures*; World Scientific Pub.: Hackensack, NJ, 2012.
(45) Kreibig, U.; Vollmer, M. *Optical Properties of Metal Clusters*; Springer: Berlin; New York, 1995.
(46) Morales, D.; Stoute, N. A.; Yu, Z.; Aspnes, D. E.; Dickey, M. D. Liquid Gallium and the Eutectic Gallium Indium (EGaIn) Alloy: Dielectric Functions from 1.24 to 3.1 eV by Electrochemical Reduction of Surface Oxides. *Appl. Phys. Lett.* **2016**, *109* (9), 91905.
(47) Maldovan, M.; Bockstaller, M. R.; Thomas, E. L.; Carter, W. C. Validation of the Effective-Medium Approximation for the Dielectric Permittivity of Oriented Nanoparticle-Filled Materials: Effective Permittivity for Dielectric Nanoparticles in Multilayer Photonic Composites. *Appl. Phys. B* **2003**, *76* (8), 877–884.
(48) Dobbins, R. A.; Megaridis, C. M. Absorption and Scattering of Light by Polydisperse Aggregates. *Appl. Opt.* **1991**, *30* (33), 4747.
(49) Bombalski, L.; Dong, H.; Listak, J.; Matyjaszewsk, K.; Bockstaller, M. R. Null-Scattering Hybrid Particles Using Controlled Radical Polymerization. *Adv. Mater.* **2007**, *19* (24), 4486–4490.
(50) Narayanan, S.; Choi, J.; Porter, L.; Bockstaller, M. R. Flexible Transparent Metal/Polymer Composite Materials Based on Optical Resonant Laminate Structures. *ACS Appl. Mater. Interfaces* **2013**, 130506144010009.
(51) Hakem, I. F.; Leech, A. M.; Johnson, J. D.; Donahue, S. J.; Walker, J. P.; Bockstaller, M. R. Understanding Ligand Distributions in Modified Particle and Particlelike Systems. *J. Am. Chem. Soc.* **2010**, *132* (46), 16593–16598.
(52) Boles, M. A.; Engel, M.; Talapin, D. V. Self-Assembly of Colloidal Nanocrystals: From Intricate Structures to Functional Materials. *Chem. Rev.* **2016**, *116* (18), 11220–11289.

TOC